OPEN ACCESS
CellPress

Cell Reports
Article

Precision of Discrete and Rhythmic Forelimb Movements Requires a Distinct Neuronal Subpopulation in the Interposed Anterior Nucleus

Aloysius Y.T. Low,[1,2,3,6] Ayesha R. Thanawalla,[1,3,6] Alaric K.K. Yip,[1,2,3,6] Jinsook Kim,[4] Kelly L.L. Wong,[1,3] Martesa Tantra,[1,3] George J. Augustine,[4,5] and Albert I. Chen[1,3,5,7,*]

[1]Nanyang Technological University (NTU), School of Biological Sciences, Singapore 637551, Singapore
[2]NTU Institute for Health Technologies, Interdisciplinary Graduate School, Singapore 637553, Singapore
[3]University of Warwick, School of Life Sciences, Coventry CV4 7AL, UK
[4]Lee Kong Chian School of Medicine, NTU, Singapore 308232, Singapore
[5]A*STAR, Institute of Molecular and Cell Biology, Singapore 138673, Singapore
[6]These authors contributed equally
[7]Lead Contact
*Correspondence: albert.chen@ntu.edu.sg
https://doi.org/10.1016/j.celrep.2018.02.017

SUMMARY

The deep cerebellar nuclei (DCN) represent output channels of the cerebellum, and they transmit integrated sensorimotor signals to modulate limb movements. But the functional relevance of identifiable neuronal subpopulations within the DCN remains unclear. Here, we examine a genetically tractable population of neurons in the mouse interposed anterior nucleus (IntA). We show that these neurons represent a subset of glutamatergic neurons in the IntA and constitute a specific element of an internal feedback circuit within the cerebellar cortex and cerebello-thalamo-cortical pathway associated with limb control. Ablation and optogenetic stimulation of these neurons disrupt efficacy of skilled reach and locomotor movement and reveal that they control positioning and timing of the forelimb and hindlimb. Together, our findings uncover the function of a distinct neuronal subpopulation in the deep cerebellum and delineate the anatomical substrates and kinematic parameters through which it modulates precision of discrete and rhythmic limb movements.

INTRODUCTION

The cerebellum is a critical component of the CNS, involved in sensorimotor integration and voluntary motor adaptation (Eccles et al., 1967; Ito, 2006). Sensory information conveying various modalities, as well as vestibular and proprioceptive information, is relayed to the cerebellum through afferent pathways (Alstermark and Ekerot, 2013; Bostan et al., 2013). The cerebellum also receives efference copy signals from motor centers and the spinal cord, and it is thought to contribute to the generation of feedforward motor commands during movement (Azim et al., 2014a; Franklin and Wolpert, 2011). Thus, a myriad of motor and sensory information from internal and external sources are known to be processed by the cerebellum. However, the circuits through which the cerebellum conveys this integrated information to relevant brain centers and within itself in the context of complex, goal-directed limb movement are not well understood.

Neurons in the deep cerebellar nuclei (DCN) provide the cerebellum with the capability of influencing motor output by linking the cerebellum with many regions of the brain (Bostan et al., 2013). The DCN is broadly subdivided into the lateral, interposed (Int), and medial nuclei in rodents, and each nucleus contains nucleocortical (NC) efferents, which provide a source of mossy fibers (MFs) in the cerebellar cortex and nucleofugal (NF) efferents, which target extra-cerebellar regions (Chan-Palay, 1977; Tolbert et al., 1978). Based on morphological, molecular, and electrophysiological distinctions, at least six neuronal subtypes have been identified in the DCN consisting of glutamatergic, γ-aminobutyric acid-ergic (GABAergic) and/or glycinergic interneurons and projection neurons (Chan-Palay, 1977; Uusisaari and Knöpfel, 2011). However, with the exceptions of a subclass of NC neurons (Ankri et al., 2015; Gao et al., 2016) and neurons that project to the vestibular nuclei (Bagnall et al., 2009) and olivary nuclei (Lefler et al., 2014), the molecular identity of efferents linking the DCN to ascending brain targets is not well defined. Moreover, details of the precise target zone and organization principles are lacking because of the challenges of isolating individual neuronal subpopulations in the DCN.

As the major output neurons in the cerebellum, DCN neurons receive input from Purkinje cells, which are innervated by granule cells that receive a convergence of sensory and motor signals (Chan-Palay, 1977; De Schutter and Bjaalie, 2001), and input from collaterals of MFs and climbing fibers (Najac and Raman, 2017; Uusisaari and De Schutter, 2011). Thus, signals arising from the DCN represent a unique convergence of inputs to the cerebellum and may play an essential role in cerebellar computation. The Int nucleus is implicated in reaching and grasping in humans and monkeys, as well as in bending of limbs and paw placement during locomotion in cats (Armstrong and Edgley,

1984; Bracha et al., 1999; Küper et al., 2011; Monzée et al., 2004). Optogenetic studies provide evidence that the Int nucleus also controls motor learning and kinematics of the eyelid (Gao et al., 2016; Heiney et al., 2014) and mediates forelimb movements through Purkinje cell activities (Lee et al., 2015; Witter et al., 2013). These studies suggest that the Int nucleus has the ability to influence motor output; however, the circuit elements through which Int neurons exert their activities have not been defined. Moreover, the requirements and the contribution of individual cell types within the Int nucleus to rhythmic and discrete movement have not been sufficiently addressed.

In this study, we examine the molecular identity, connectivity, and function of a subpopulation of neurons in the mouse DCN. We discover the utility of *urocortin 3* (*Ucn3*)::Cre mouse line for labeling, monitoring, and manipulating *Ucn3*::Cre-recombined neurons in the IntA nucleus (IntA^{Ucn3}). We provide electrophysiological and molecular evidence that IntA^{Ucn3} neurons represent a subset of glutamatergic neurons in the IntA. Using a combination of genetic and viral tracing strategies, we show that IntA^{Ucn3} neurons give rise to nucleocortical mossy fibers (NC-MFs) that preferentially target a specific forelimb-related region of the cerebellar cortex and primarily project to a highly restricted region of the motor thalamus linked to the caudal forelimb area of the motor cortex. Diphtheria toxin-mediated ablation and optogenetic stimulation of IntA^{Ucn3} neurons disrupt skilled reach and locomotion by influencing limb positioning and timing. Our findings describe a subpopulation of glutamatergic projection neurons in the deep cerebellum that regulates the precision of complex, goal-directed limb movements, perhaps by providing feedback signals to the cerebellar cortex and modifying motor commands through the cerebello-thalamo-cortical pathway.

RESULTS

Selective Genetic Targeting of a Subpopulation of Glutamatergic Neurons in the IntA

To define connectivity and function of neuronal subpopulations in the DCN, we identified and acquired a bacterial artificial chromosome transgenic mouse line *Ucn3*::Cre, which mediates recombination in DCN neurons (Gene Expression Nervous System Atlas [GENSAT]; Mutant Mouse Regional Center). We assessed the recombination ability of *Ucn3*::Cre mice by crossing them with *Rosa26*::lsl-eGFP (enhanced green fluorescent protein) and *Rosa26*::lsl-Channelrhodopsin (ChR2)-eYFP (enhanced yellow fluorescent protein) mice (*Rosa*::ChR2) and found recombined neurons in the Int nucleus (Figure 1A). Using the nine subnuclei defined by histological distinctions (Figures 1B and S1A–S1D) (Paxinos and Franklin, 2007), we found that recombined neurons are concentrated within the IntA and sparsely distributed in other regions (Figures 1C–1E). Quantification of their distribution indicates that >70% of total YFP^{+} neurons in the DCN are located in the IntA, with 15% in the medial nucleus and ~15% in the remaining five subnuclei (Figure 1F; Table S1).

To determine the electrophysiological properties of the IntA^{Ucn3} neurons, we made patch-clamp measurements of the intrinsic electrical properties of YFP^{+} IntA^{Ucn3} neurons (YFP^{ON}) and YFP^{-} non-IntA^{Ucn3} neurons (YFP^{OFF}). YFP^{ON} neurons had a higher firing rate than most YFP^{OFF} neurons (Figures 2A and 2B). In addition, we found some YFP^{OFF} neurons with a firing rate similar to that of YFP^{ON} neurons (Figures 2A and 2B). These values are in the range of firing rates of glutamatergic neurons in the DCN (Uusisaari et al., 2007). Analysis of the diameter and area further subdivides these neurons into three groups (large YFP^{ON} [YFP^{ON}-L], large YFP^{OFF} [YFP^{OFF}-L], and small YFP^{OFF} [YFP^{OFF}-S]). YFP^{ON}-L and YFP^{OFF}-L neurons are approximately four times larger in area and approximately two times larger in diameter than YFP^{OFF}-S neurons (Figure 2C). Although the distribution of soma sizes of non-GABAergic and GABAergic neurons is overlapping, a soma size greater than 300 μm^2 in area and 25 μm in diameter is indicative of non-GABAergic neurons in the DCN (Uusisaari et al., 2007). Analysis of the intrinsic electrical properties, including those previously described, revealed no significant differences between the properties of YFP^{ON}-L and YFP^{OFF}-L neurons (Figures 2B and S1J–S1N) (Uusisaari et al., 2007). However, there are significant differences between YFP^{ON}-L and YFP^{OFF}-S neurons, including input resistance, membrane capacitance, action potential (AP) half-width, and AP frequency (Figures 2B and S1J–S1N). Thus, of the six neuronal cell types described in the DCN (Uusisaari and Knöpfel, 2011), we have determined that IntA^{Ucn3} neurons belong to a class of large glutamatergic neurons. In addition, the presence of YFP^{OFF}-L neurons indicates that the IntA^{Ucn3} neurons comprise a subset of glutamatergic neurons in the IntA.

To define molecular distinctions of IntA^{Ucn3} neurons, we assessed whether YFP^{ON} neurons express glutamatergic molecular markers (vGluT2, SMI32, and T-box brain 1 [TBR1]) or GABAergic molecular markers (GAD67, Calretinin, and Tfap2A) (Chung et al., 2009; Leto et al., 2006; Zainolabidin et al., 2017). We found that IntA^{Ucn3} neurons express vGluT2, SMI32, and TBR1, but not GAD67, Calretinin, or Tfap2A (Figures 2D–2F, 2H–2J, and 2K–2Y; Table S1). Even though TBR1 colocalizes with IntA^{Ucn3} neurons (TBR1^{+}YFP^{ON}/YFP^{ON} = 99% ± 1%), the level of TBR1 expression is lower in the IntA compared to the medial nucleus, consistent with previous descriptions (Figures S1E–S1I) (Chung et al., 2009). IntA^{Ucn3} neurons make up ~45% of all vGluT2^{+} presumptive glutamatergic neurons in the IntA (Figure 2G). Thus, using *Ucn3*::Cre mice, we are able to selectively label a subpopulation of glutamatergic neurons in the IntA that have distinct electrophysiological, morphological, and molecular features. Furthermore, by characterizing the recombination ability of *Ucn3*::Cre mice, we are able to manipulate neurons defined by *Ucn3*::Cre in the cerebellum.

Intra- and Extra-cerebellar Connectivity of Neuronal Subpopulations in the IntA

IntA^{Ucn3} Neurons Send NC-MFs to a Restricted Region of the Cerebellar Cortex

To define targets of IntA^{Ucn3} neurons, we analyzed their axonal projections in *Ucn3*::Cre; *Rosa*::ChR2 mice. Even though *Ucn3*::Cre mice permit specific targeting of neurons in the IntA (Figure 1), recombination occurs in the amygdala and hypothalamus, and axons from these regions could interfere with our analysis

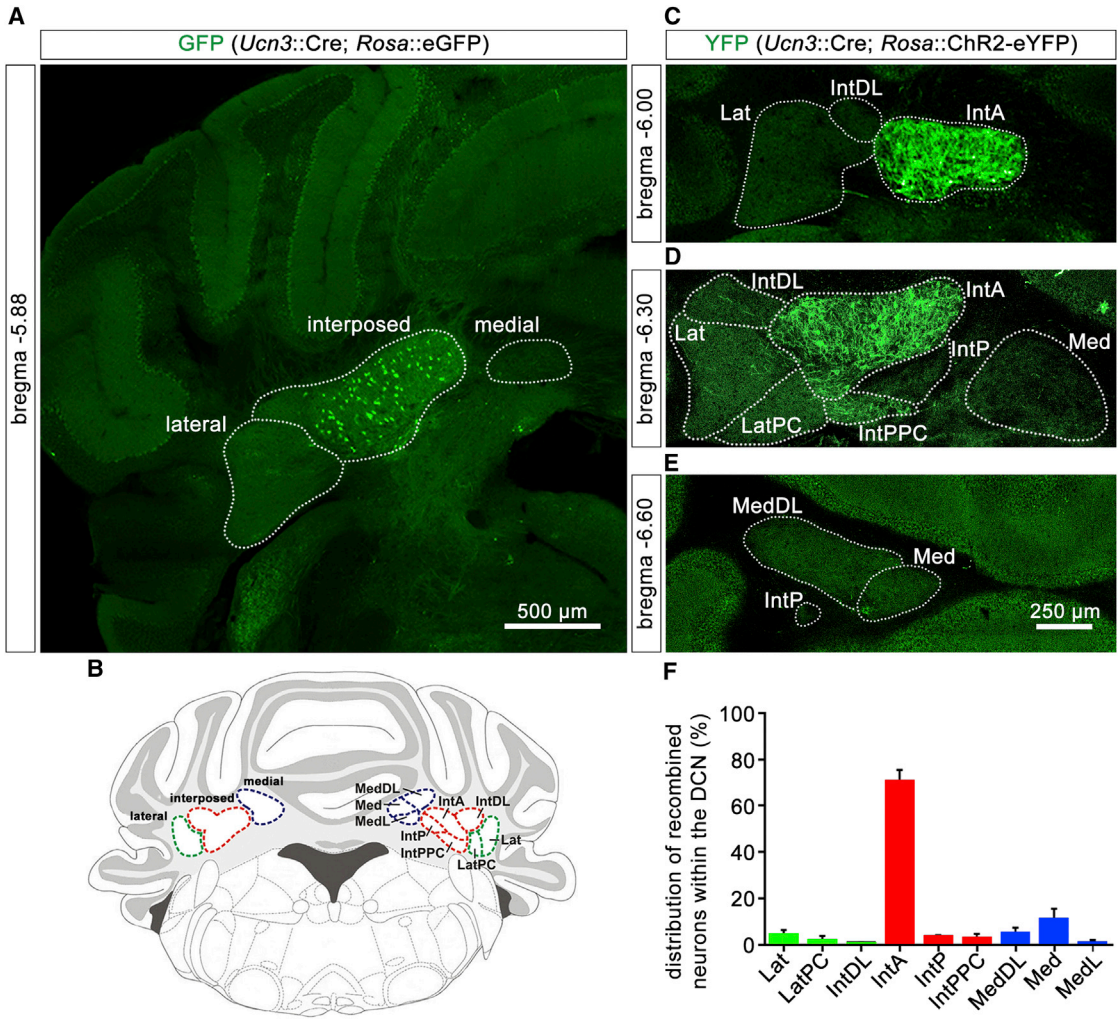

Figure 1. Selective Genetic Targeting of Neurons in the IntA

(A) GFP expression in the Int of the DCN in coronal sections from a *Ucn3*::Cre; *Rosa*::eGFP mouse.

(B) Schematic of the three major nuclei and nine subdivisions in the DCN.

(C–E) Within each subdivision, YFP is detected primarily in the IntA of a *Ucn3*::Cre; *Rosa*::ChR2 mouse (C) and (D), but not in the other subnuclei (C)–(E).

(F) Quantification of the distribution of YFP$^+$ neurons in each of the subdivisions of *Ucn3*::Cre; *Rosa*::ChR2 mice.

Lat, lateral; LatPC, lateral parvicellular; IntDL, interposed dorsolateral; IntA, interposed anterior nucleus; IntP, interposed posterior; IntPPC, interposed posterior parvicellular; MedDL, medial dorsolateral; Med, medial; MedL, medial lateral. Mean ± SEM; n = 2,617, 2,180, and 4,406 neurons. Age of mice: P56–P63.

(Shemesh et al., 2016). Therefore, we injected AAV2-*hSyn*::mCherry and AAV2-*hSyn*::ChR2-mCherry into the IntA of *Ucn3*::Cre; *Rosa*::ChR2 mice to distinguish between IntA^{Ucn3} neurons (YFP$^+$mCherry$^+$, yellow) and non-IntA^{Ucn3} neurons (mCherry$^+$, red) (Figures 3A–3C). We labeled ~92% of IntA^{Ucn3} neurons with mCherry and found that IntA^{Ucn3} neurons make up ~50% of all mCherry$^+$ neurons (Table S2). Using this strategy, we were able to differentiate projections from IntA^{Ucn3} neurons and those from non-IntA^{Ucn3} neurons. However, one limitation of this double-labeling strategy is that because ~8% of IntA^{Ucn3} neurons were not labeled with mCherry, we are only able to analyze the projection patterns of most IntA^{Ucn3} neurons.

To explore potential distinctions in IntA NC connectivity, we analyzed the colocalization of NC-MFs across cortical lobules with vGluT1/2. While MFs in the internal granular layer (IGL) of the cerebellum differentially express vGluT1 and vGluT2 (Hioki et al., 2003), MFs derived from NC neurons only express vGluT2 (Gao et al., 2016). We found that NC-MFs from IntA^{Ucn3} neurons express vGluT2, but not vGluT1 (Figures 3D–3G) (data not shown). NC-MFs from IntA^{Ucn3} neurons are located primarily in the IGL of lobules IV and V and simple lobule (Sim) close to Purkinje and Golgi cell somata (Figures S2L–S2O; Table S3). Consistent with previous work, we observed a preferential targeting of NC-MFs to the Zebrin$^-$ microzone and to the superficial region in the IGL (Figures 3H–3K and S2L–S2O) (Gao et al., 2016). We observed that IntA^{Ucn3} NC-MFs show selective targeting to the anterior, but not the posterior, forelimb region based on modules defined by olivo-cortico-nuclear connectivity

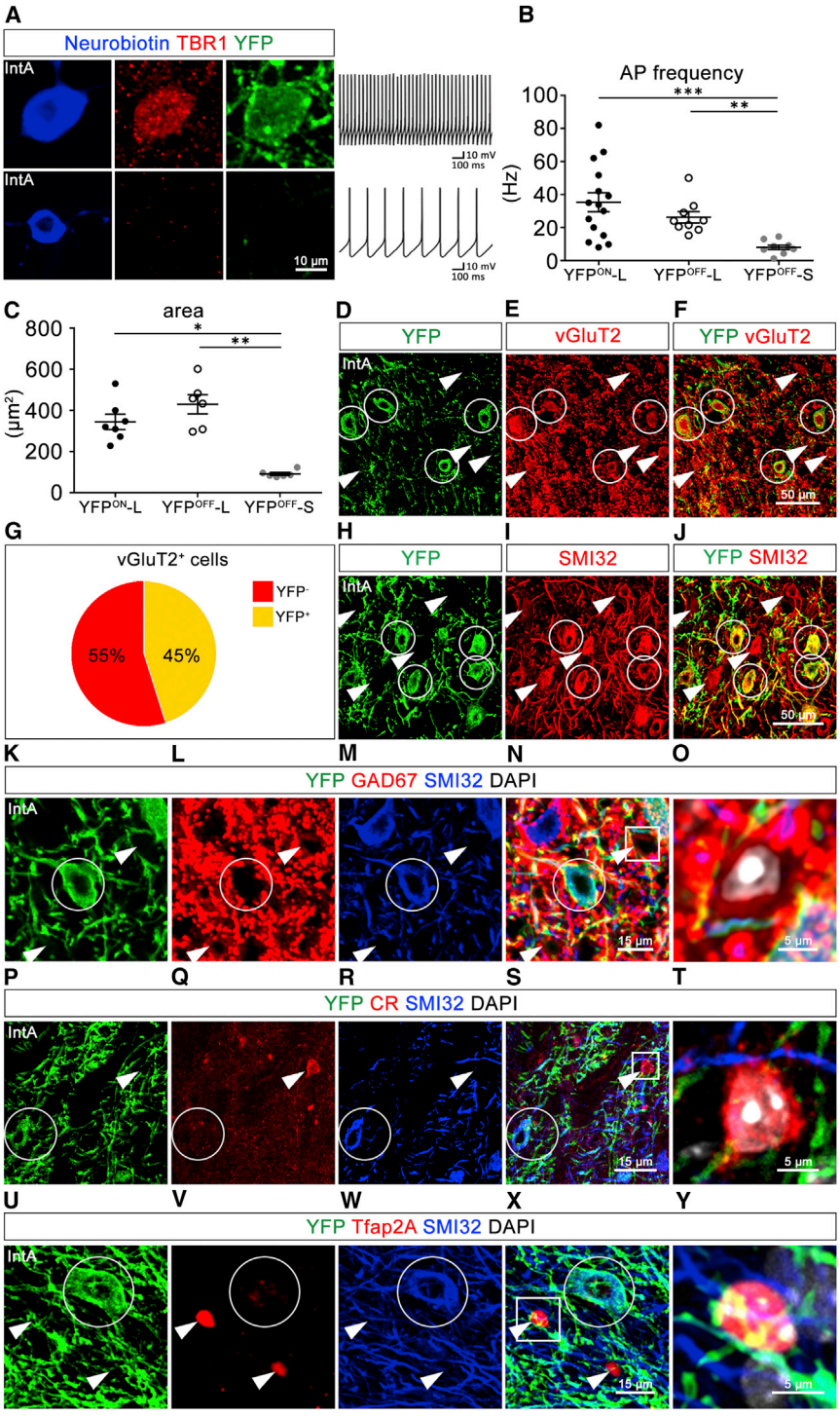

Figure 2. Identification of a Distinct Subpopulation of Glutamatergic Neurons in the IntA

(A) Combined patch-clamp recording and immunohistochemistry labeling of two neurons from the IntA of P30 *Ucn3*::Cre; *Rosa*::ChR2. Patched neurons were filled with Neurobiotin (blue) to correlate action potential firing with immunocytochemical properties. Top row shows a neuron that was YFP^{+} (green) and TBR1^{+} (red) fired spontaneously at a high rate. Bottom row shows a YFP^{-}TBR1^{-} neuron fired spontaneously at a lower rate.

(B and C) Analysis of the action potential (AP) frequency (YFP^{ON}-L, 35.4 ± 5.7 Hz; YFP^{OFF}-L, 26.3 ± 3.5 Hz; YFP^{OFF}-S, 8.1 ± 1.4) (B) and area (YFP^{ON}-L, 344.2 ± 37.15 μm^2; YFP^{OFF}-L, 430.4 ± 46.71 μm^2; YFP^{OFF}-S, 91.86 ± 6.91 μm^2) (C) among YFP^{ON}-L, YFP^{OFF}-S, and YFP^{OFF}-L neurons.

(D–J) YFP^{+} neurons in the IntA (green, D and H) express vGluT2 (red, E) and SMI32 (red, I) (merged in F and J). Percentage of YFP^{ON} (45% ± 6%) and YFP^{OFF} neurons (55% ± 4%) within vGluT2^{+} neurons (G).

(K–Y) YFP^{+} neurons in the IntA (green; K, P, and U) express SMI32 (blue; M, R, and W), but do not express GAD67 (red, L), Calretinin (red, Q), or Tfap2A (red, V) (merged in N, S, and X; DAPI, white, O, T, and Y).

Circles indicate cells with colocalization, and arrowheads indicate cells without colocalization. Mean ± SEM; n = 7–15 YFP^{ON}-L, 6–9 YFP^{OFF}-S, and 6–9 YFP^{OFF}-L neurons. *p ≤ 0.05, **p ≤ 0.01.

(Figures 3L and 3M; Table S3) (Voogd et al., 2003). These results indicate that IntA^{Ucn3} neurons comprise a subset of IntA neurons that projects to a restricted region of the cerebellar cortex distinct from other IntA neurons. Together, we introduce a genetic method to monitor and manipulate a subpopulation of IntA NC neurons that has been implicated in amplification of efference copy signals (Beitzel et al., 2017; Gao et al., 2016; Houck and Person, 2015).

IntA^{Ucn3} Neurons Send Extensive Projections to the VA-VL Thalamus Linked to the CFA of M1

We next analyzed the targets of IntA^{Ucn3} neurons by comparing the extracerebellar projection patterns of IntA^{Ucn3} and non-IntA^{Ucn3} neurons with projections from all IntA neurons. Labeled puncta in target regions colocalize with vGluT2, except in the dorsal nucleus of the inferior olivary complex (IOD), indicating that they represent synaptic terminals (Figure S3). The terminal distribution patterns in six regions traced from distinct subpopulations of neurons are converted into a heatmap coding for minimum and maximum percentage values and organized from lowest to highest incidence of puncta (Figures 4A and S3; Table S4). Even though both IntA^{Ucn3} and non-IntA^{Ucn3} neurons project to the same regions, puncta originating from each population are differentially distributed (Figures 4A and S3). In the descending pathway, toward the brain stem, we found sparse mCherry^{+} puncta in the IOD and Lateral reticular nucleus (LRt), consistent with studies in the cat (Figures S3A and S3B,

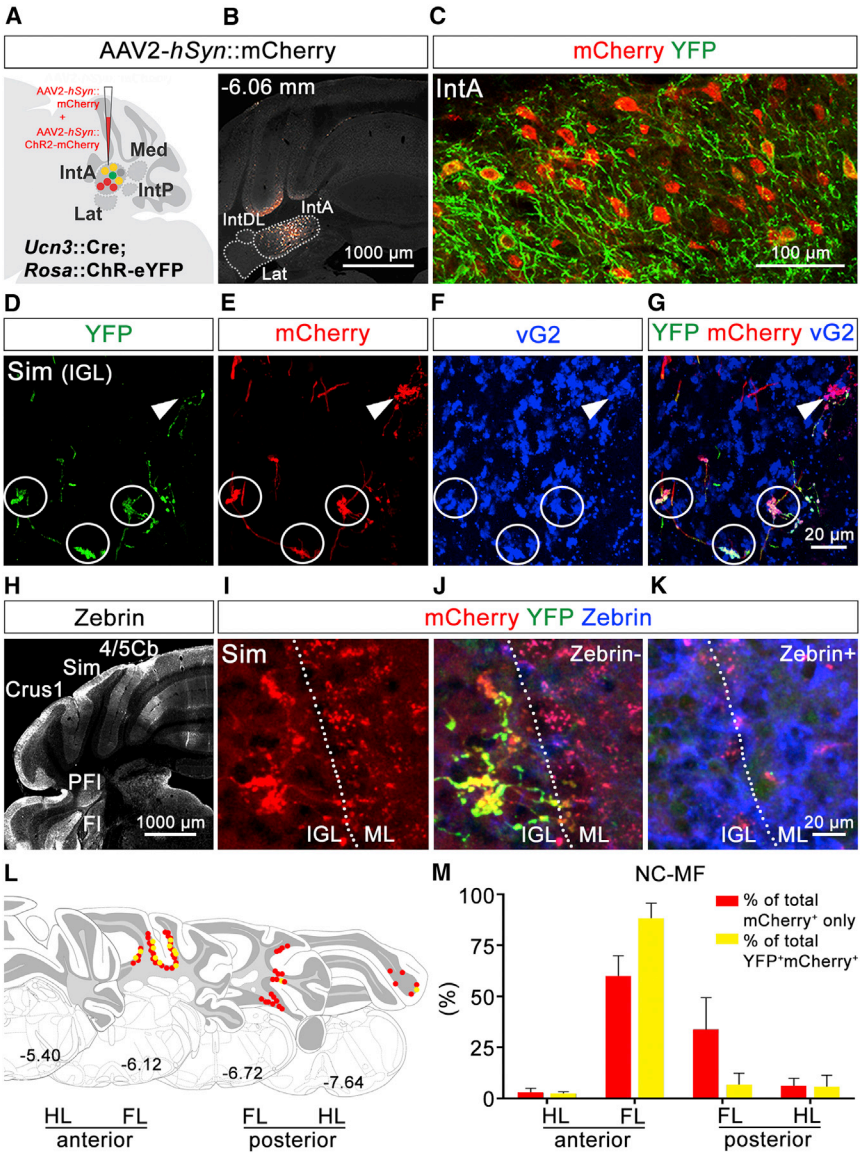

Figure 3. IntA^{Ucn3} Neurons Give Rise to NC-MFs Restricted to the Anterior Forelimb-Associated Region

(A) Strategy for tracing the projections of IntA^{Ucn3} neurons (yellow) versus other IntA neurons (red).

(B) Expression of mCherry in the IntA of a *Ucn3*::Cre; *Rosa*::ChR2 mouse after transduction with AAV2-*hSyn*::mCherry and AAV2-*hSyn*::ChR2-mCherry.

(C) Most YFP$^+$ neurons (green) in the IntA are mCherry$^+$ (red).

(D–G) YFP$^+$ and YFP$^-$ NC-MFs (green, D) within the IGL of the simple lobule (Sim) express mCherry (red, E) and vGluT2 (vG2; blue, F) (merged in G).

(H–K) Zebrin staining (H) shows mCherry$^+$ (red, I) and YFP$^+$ (green, J) NC-MFs are located in the Zebrin$^-$ microzone (J), but not in the Zebrin$^+$ microzone (K), in the IGL of the simple lobule.

(L) Distribution of non-IntA^{Ucn3} and IntA^{Ucn3} NC-MFs across coronal planes of the cerebellum at the indicated bregma points in forelimb- and hindlimb-associated regions (Voogd et al., 2003).

(M) Quantification of the distribution of non-IntA^{Ucn3} (red) and IntA^{Ucn3} (yellow) NC-MFs as a percentage of total number of respective rosettes across all cerebellar lobules.

Circles indicate cells with colocalization, and arrowheads indicate cells without colocalization. Mean ± SEM. Age of mice: P56–P63. See Figure S2 and Tables S2 and S3.

IOD; Figures S3G and S3H, lateral reticular nucleus; Table S4) (Teune et al., 2000). Less than 15% of total mCherry puncta were found in each of these two regions; furthermore, a scant ~25% of these mCherry$^+$ puncta in the IOD and LRt belonged to IntA^{Ucn3} neurons (Figures 4A and S3; Table S4).

Next, we assessed the projections in brain regions in the ascending pathway, toward the midbrain and forebrain. We observed mCherry puncta on the contralateral side in the magnocellular portion of the red nucleus (RN) (red nucleus magnocellular part [RMC]) (Figures S3I and S3J), intermediate gray layer of the superior colliculus (InG) (Figures S3E and S3F), ventral part of the zona incerta (ZIV) (Figures S3C and S3D), and the ventral anterior-ventral lateral (VA-VL) thalamus (Figures S3K–S3S). The Int nucleus sends extensive projections to the RN and the VA-VL (Teune et al., 2000). Consistently, >50% of all mCherry$^+$ puncta are found in the RMC and VA-VL (Figure 4A; Table S4). When these puncta are separated into IntA^{Ucn3} puncta (mCherry$^+$/YFP$^+$, yellow) and non-IntA^{Ucn3} puncta (mCherry$^+$/YFP$^-$, red), we find a greater proportion of IntA^{Ucn3} puncta within the VA-VL (Figure 4A; Table S4). Our genetic and viral tract tracing results reveal that neurons in the IntA differentially project to distinct extra-cerebellar targets and that the IntA^{Ucn3} neurons preferentially project toward the VA-VL.

To map the contribution of IntA^{Ucn3} neurons to the cerebello-thalamo-cortical pathway, we analyzed the termination site within molecular and morphological distinct subregions of the VA-VL (Figure 4B) (Kuramoto et al., 2011). The VA-VL is subdivided into a region containing a high density of large vGluT2 puncta (vGluT2^L) and a region containing a low density of small vGluT2 puncta (vGluT2^S) (Figures 4H, S3L, and S3P) (Kuramoto et al., 2011). In addition, Calbindin (CB) is expressed by neurons in the vGluT2^S region and in a small zone within the vGluT2^L region (Figures 4E and 4J) (Kuramoto et al., 2011). We observed a high coincidence of puncta from IntA^{Ucn3} neurons in the CB$^-$ region (Figures 4C–4F). Moreover, we observed that these terminals reside in a subregion of the vGluT2^L and CB$^-$ zone (Figures 4G–4J).

Because neurons in the vGluT2^L CB$^-$ zone send extensive projections to the motor and sensory cortex (Kuramoto et al., 2009, 2011), we injected cholera toxin subunit B (CTB) conjugated with fluorophore-555 into the caudal forelimb area (CFA) of the M1 region (Figures 4K and 4L) (Tennant et al., 2011). In the VA-VL on the ipsilateral side, we observed CTB-555$^+$ somata

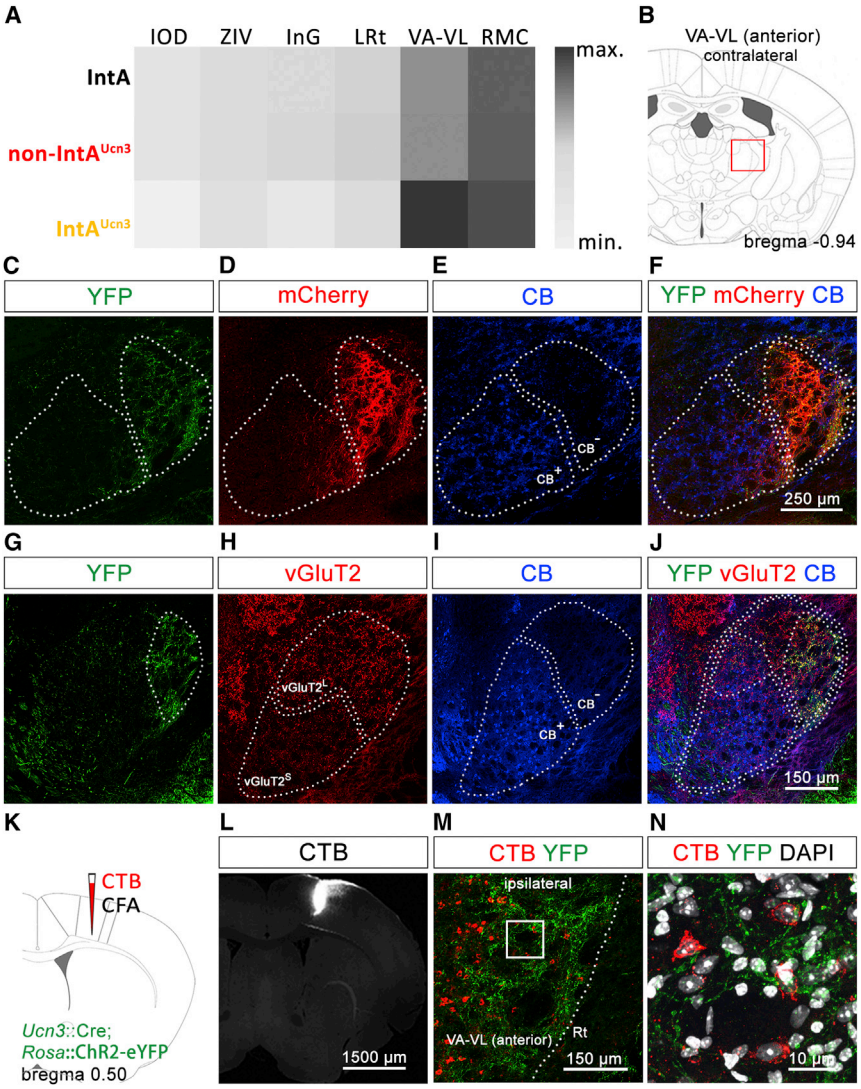

Figure 4. IntA^{Ucn3} Neurons Constitute a Specific Element of the Cerebello-Thalamo-Cortical Network

(A) Heatmap of the relative distribution of traced puncta from IntA^{Ucn3} neurons (YFP^{+}mCherry^{+}, yellow) and other IntA neurons (YFP^{-}mCherry^{+}, red) to six major regions.

(B) Schematic of thalamic region with puncta from IntA^{Ucn3} neurons. The red box denotes the VA-VL subregion.

(C–F) Puncta from IntA^{Ucn3} neurons that express both YFP (green, C) and mCherry (red, D) terminate outside the CB^{+} region (blue, E) in the anterior VA-VL (merged in F).

(G–J) YFP^{+} fibers (green, G) are found in a subregion of the vGluT2^{L} (red, H) and CB^{-} (blue, I) zone (merged in J).

(K and L) Retrograde CTB injection site in the CFA (K, schematic; L, white).

(M) CTB^{+} cell bodies (red) overlap in the anterior VA-VL region containing fibers from IntA^{Ucn3} neurons (green).

(N) Magnified region from the white box in (M) (DAPI, white).

Age of mice: P56–P63. See Figure S4 and Table S4.

close to YFP^{+} fibers from IntA^{Ucn3} neurons (Figures 4M and 4N), suggesting that IntA^{Ucn3} neurons form contacts with neurons projecting into the forelimb motor command center of the cortex (Tennant et al., 2011). We have not determined whether IntA^{Ucn3} neurons that make up the NC-MF pathway are the same neurons as those that make up the cerebello-thalamo-cortical pathway. Thus, our mapping analysis indicates that IntA^{Ucn3} neurons have a distinct intra- and extra-cerebellar connectivity pattern compared to non-IntA^{Ucn3} neurons. Moreover, we define specific downstream circuit elements that could serve as substrate for IntA^{Ucn3} neurons to mediate complex and coordinated responses for limb movement and locomotion.

Consequences of the Ablation of IntA^{Ucn3} Neurons on Discrete and Rhythmic Forelimb Movement

Ablation of IntA^{Ucn3} Neurons Perturbs the Accuracy of Skilled Forelimb Reaching

To assess the requirement of IntA neurons targeted by *Ucn3*::Cre mice in mediating limb movements, we used a chemogenetic method to selectively eliminate these neurons. Conventional deletion of *Ucn3* results in amygdala-dependent social deficits without disrupting general motor activities (Shemesh et al., 2016). We unilaterally injected AAV2-*EF1a*::double-floxed-DTR-eGFP into the DCN of *Ucn3*::Cre reporter mice (Figures 5A and S4C). One to two weeks after injection, a subset of TBR1^{+} IntA neurons expressed diphtheria toxin receptor (DTR)-eGFP (Figures 5B and S4C–S4E). We administered diphtheria toxin (DT) 21 days after the initial injection of the virus and observed a ~30% reduction in number of TBR1^{+} neurons 7–21 days after DT treatment, indicating near-complete elimination of IntA^{Ucn3} neurons in the IntA (Figures 5B and S4F–S4H). To address potential perturbation in gross motor coordination, IntA^{Ucn3}-ablated mice were tested in the open field and on the rotating rod. The total distance traveled and average velocity in the open field, as well as performance on the rotating rod, were comparable in ablated mice compared to control (Figures S4I–S4K).

To explore the involvement of IntA^{Ucn3} neurons in discrete forelimb movements on the ipsilateral side of ablation, we trained mice in a staircase reaching task (Figure 5C) (Klein and Dunnett, 2012). The staircase reaching task is similar to the single-pellet reaching task for assessment of the ability and kinematics of skilled reaching in mice (Klein and Dunnett, 2012). We found that ablated mice were less successful at acquiring food pellets compared to control (Figure 5D; Movies S1 and S2). To assess which aspects of skilled reach is affected by the ablation, we categorized the task into reach, grasp, and retrieve phases

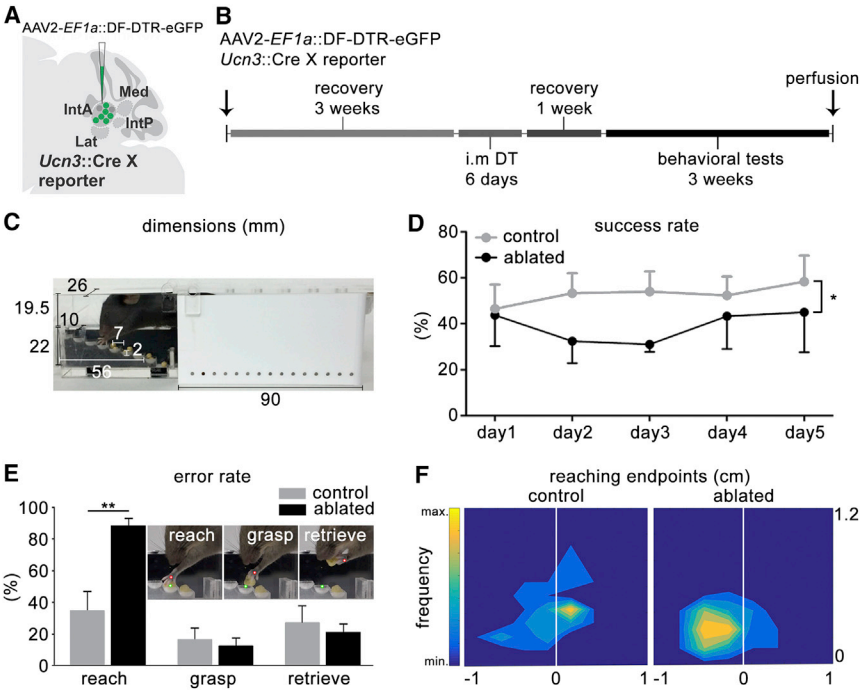

Figure 5. Ablation of IntA^{Ucn3} Neurons Disrupts the Accuracy of Forelimb-Skilled Reaching

(A) Strategy for the selective ablation of IntA^{Ucn3} neurons.

(B) Timeline for ablation and behavioral experiments.

(C) Image and dimensions of the staircase.

(D) Success rate (as a percentage) in staircase skilled reaching of control and IntA^{Ucn3}-ablated mice (control [cont.] overall: 53 ± 2, ablated: 39 ± 3, two-way ANOVA, p = 0.016).

(E) Phases of reaching (insets). Error rate (as a percentage) of control and ablated mice (reach, cont.: 37 ± 13, ablated: 88 ± 5, p = 0.0025; grasp, cont.: 16 ± 8, ablated: 12 ± 5, p = 0.985; retrieve, cont.: 27 ± 11, ablated: 20 ± 6, p = 0.956).

(F) Reaching endpoints of ablated mice (pellet position indicated by the white line) (cont. xy: 0.06 ± 0.06, 0.394 ± 0.03; ablated xy: −0.133 ± 0.06, 0.314 ± 0.03; p = 0.003).

Mean ± SEM; cont.: n = 8 animals, ablated: n = 10 animals. See Figure S5.

and analyzed each separately (Figure 5E, inset). We discovered that ablated mice exhibited a greater than two-fold increase in reaching errors compared to control, but their abilities to grasp and retrieve food pellets were unaffected (Figure 5E).

To examine the positioning of forelimb movement during the reaching phase in more detail, we plotted the endpoints relative to the pellet in the *xy* plane of their reach attempts and the angle between the paw and the pellet. We found that control mice reach for the pellet in a near-straight path directly on top of the pellet, with errors evenly distributed between under- and overreach (Figure 5F; Movie S1). Ablated mice, however, reached farther before retrieving the pellet (Figure 5F; Movie S2). Quantification of the angle of deviation of the paw from the pellet during the reach phase reveals that while control mice show close to zero deviation from the pellet, ablated mice show ~25° deviation from the pellet in the overreach direction (Figure S4L). The position and angle of the animal's nose during reach were comparable between IntA^{Ucn3}-ablated and control mice, indicating both groups positioned themselves similarly (Figure S4M) (data not shown). Thus, ablation of IntA^{Ucn3} neurons appears to disrupt accuracy of reaching a target, while other aspects of prehension remain unaffected. Moreover, loss of IntA^{Ucn3} neurons results in mistargeting of the forelimb past the intended goal, indicating a requirement of these neurons in accurate limb positioning.

Ablation of IntA^{Ucn3} Neurons Perturbs the Timing of Locomotor Movement

To determine whether IntA^{Ucn3} neurons similarly control forelimb positioning in rhythmic movement, control and IntA^{Ucn3}-ablated mice were tested in a directed locomotor task, and the movement kinematics of only the ipsilateral forelimb were analyzed in detail across each stride. We designed and built a transparent corridor that restricts movement of mice in only one direction (Figure 6A). Mouse limb stride during locomotion can be divided into a stationary stance phase and a dynamic swing phase (Figure 6B) (Machado et al., 2015). Based on flexion and extension at the wrist joint reported in cats (Engberg and Lundberg, 1969), we further divided the swing phase into swing-flex and swing-extend (Figure 6B).

To investigate the role of IntA^{Ucn3} neurons in paw positioning during locomotion, we traced trajectories of the paw across the swing phase of the stride (Figure 6C). Along the horizontal axis, *x* displacement (Δ*x*) of the paw for each stride was consistent between control and ablated mice, indicating that paw placement at the end of each stride is conserved in the absence of IntA^{Ucn3} neurons (Figure 6D). Furthermore, Δ*x* over time remained unchanged, indicating that movement along the horizontal axis throughout the duration of the stride is maintained (Figure 6E). When plotted over time, we observed that *y* positioning is affected in the initial component of the swing phase, resulting in an aberrant pattern of walking, although the changes in *y* displacement at different stages of the swing phase did not reach statistical significance (Figures 6C and 6G–6I).

Because changes in the position of the limb during a stride could, in principle, be influenced by changes in the timing of the movement, we next compared the duration of the strides between control and ablated mice. We found that ablated mice take significantly less time to complete each stride (Figure 6J). When the stance and swing phases were analyzed separately, we found that time spent in the stance phase was significantly lower, resulting in an increase in cadence (Figures 6K–6M). The time spent in the earlier swing-flex phase is also reduced in the ablated mice (Figure S4O). These results indicate that IntA^{Ucn3} neurons are required for timing of movements necessary for the progression through distinct phases of the stride. Changes in timing of the stride result in an overall increase in cadence,

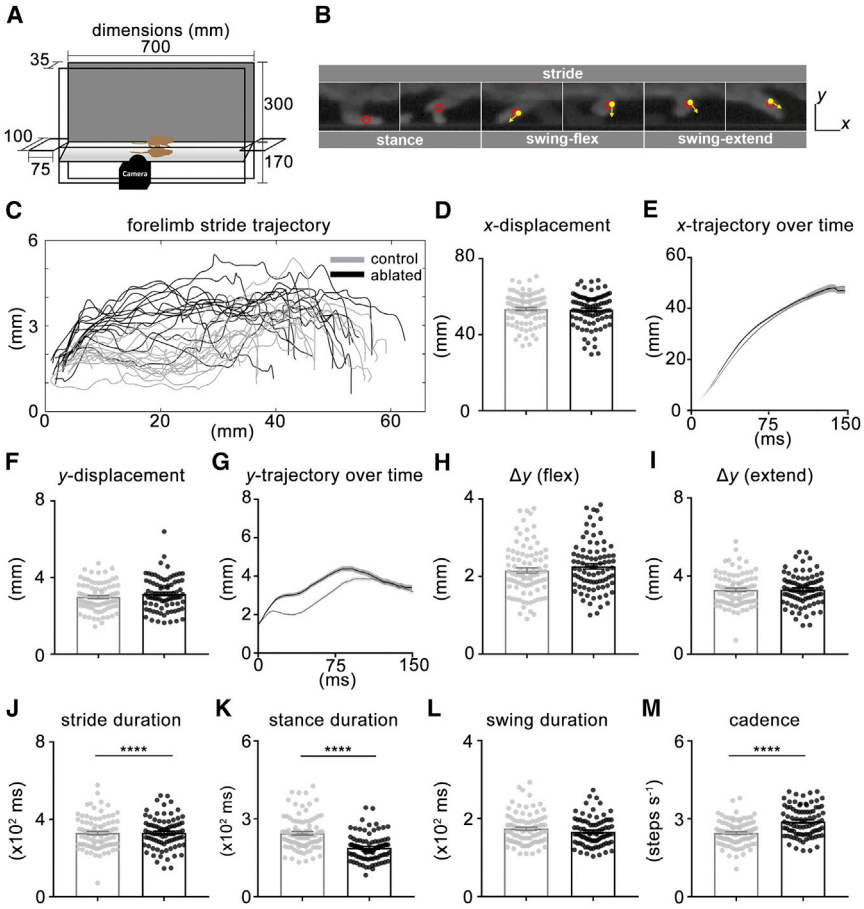

Figure 6. Ablation of IntA^{Ucn3} Neurons Perturbs the Duration of Stride in Freely Walking Mice

(A) Schematic and dimensions of the locomotor behavioral paradigm.

(B) Stride can be divided into the stance phase and the swing phase, with the swing phase further divided into swing-flex and swing-extend (Engberg and Lundberg, 1969; Machado et al., 2015).

(C) Two-dimensional traces of stride trajectory from a control (gray) and an IntA^{Ucn3}-ablated mouse (black).

(D–G) Analysis of x displacement (Δ*x*) of the paw per stride in millimeters (D) and Δ*x* over time (E), as well as analysis of y displacement (Δ*y*) from platform per stride in millimeters (F) and Δ*y* over time (G).

(H and I) Analysis of Δ*y* for the swing-flex phase (H) and the swing-extend phase (I).

(J–L) Analysis of the stride (J), stance (K), and swing duration (L) in milliseconds.

(M) Analysis of cadence.

Each point indicates a single stride. Cont.: n = 3 animals, ablated: n = 3; 25–30 strides/animal. See Figure S5 and Table S5.

which influences the rhythmicity of locomotion. We observed consistent changes in hindlimb kinematics of ablated mice, indicating that IntA^{Ucn3} neurons may directly, or indirectly, regulate aspects of the hindlimb (Figures S4U–S4X). Together, results from ablation of IntA^{Ucn3} neurons indicate that they regulate the timing of forelimb movement and stride trajectory and are required for precision of both discrete and rhythmic movement.

Photostimulation of IntA^{Ucn3} Neurons Disrupts the Positioning of Forelimb Movement during Locomotion

Acute manipulation of Purkinje cells in the simple lobule drives limb movement, presumably through influences on multiple neuronal subtypes in both Int and medial nuclei (Lee et al., 2015; Witter et al., 2013), but whether direct manipulation of a specific neuronal population in the IntA regulates limb movement has not yet been examined. Because we observed that ablation of IntA^{Ucn3} neurons disrupts specific forelimb kinematic parameters during locomotion, we set out to assess how stimulation of these neurons might influence these same parameters. We expressed ChR2 selectively in IntA neurons by generating *Ucn3*::Cre; *Rosa*::ChR2 mice and assessed the photoexcitability of ChR2-expressing IntA^{Ucn3} neurons in cerebellar slices. Upon light stimulation, ChR2-eYFP glutamatergic neurons, but not presumptive GABAergic neurons, increased their firing frequency more than two-fold (Figures S5A–S5D, normalized frequency). To assess the behavioral consequence of stimulating IntA^{Ucn3} neurons, we delivered light through optical fibers unilaterally implanted in the DCN and analyzed the effect of photostimulation on kinematics of the ipsilateral forelimb using the locomotor task described earlier (Figures 6A and 6B).

We recorded mice walking through the corridor during photostimulated and non-photostimulated trials (Movies S3 and S4). Stimulation of IntA^{Ucn3} neurons at 1, 5, and 20 Hz (1–10 mW) did not result in forelimb movement in mice at rest, indicating that under the conditions examined, IntA^{Ucn3} neurons do not appear to have the ability to initiate forelimb movement (data not shown). We also did not observe changes in forelimb movement in photostimulated trials of *Rosa*::ChR2 control mice (data not shown). A closer examination of the individual strides shows that the forelimb trajectories were modified during stimulation (Figure 7C). While we found no significant difference in Δ*x*, similar to IntA^{Ucn3}-ablated mice, we saw a >50% increase in *y* displacement (Δ*y*) (Figures 7D and 7F). In addition, when plotted over time, only Δ*y* is affected (Figures 7E and 7G). Analysis of the swing-flex and swing-extend phases revealed a significant increase in both phases (Figures 7H and 7I). In contrast to the phenotype in which the forelimb of IntA^{Ucn3}-ablated mice prematurely reached its maximum height, stimulation of IntA^{Ucn3} neurons results in an increase in Δ*y* in both swing-flex and swing-extend phases (Figures 7H, 7I, and S4R). Moreover, the resulting maximum height of the forelimb after photostimulation is greater than without it (Figure S5I). Analysis of the onset of stimulation at different stride phases revealed that the onset of stimulating IntA^{Ucn3} neurons during

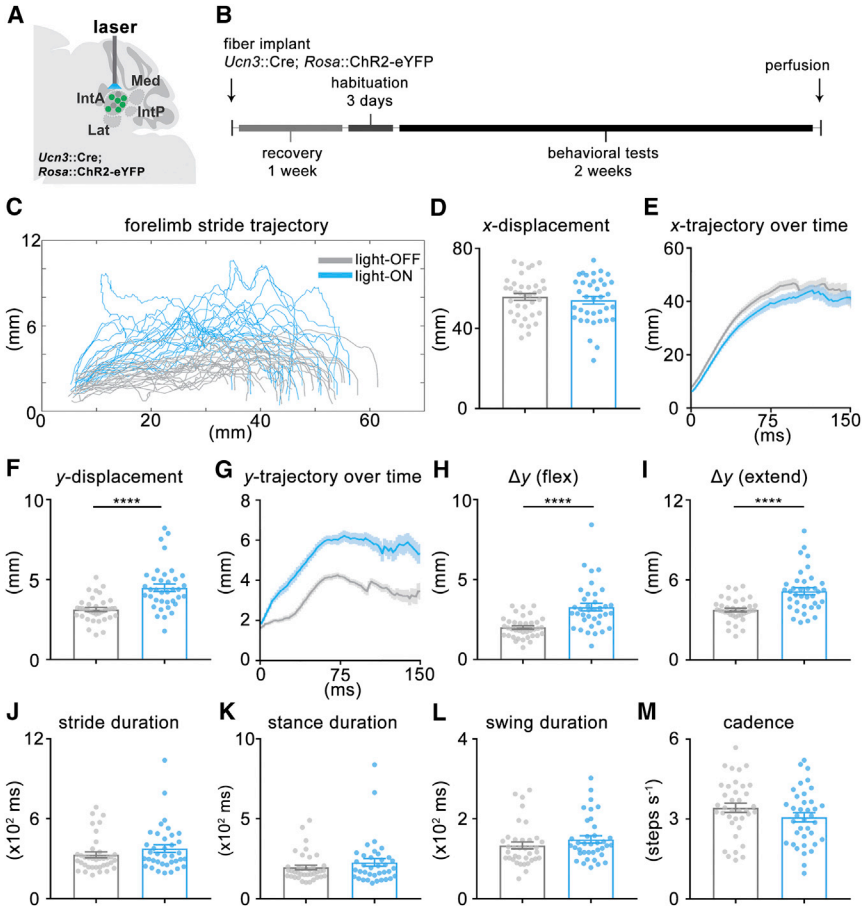

Figure 7. Photostimulation of IntA^{Ucn3} Neurons Alters the Vertical Extent of the Forelimb in Freely Walking Mice

(A and B) Strategy (A) and timeline (B) for optogenetic stimulation of IntA^{Ucn3} neurons.

(C) Two-dimensional traces of stride trajectory from a mouse with the light off (gray) and the light on (blue).

(D–G) Analysis of the Δx of the paw per stride in millimeters (D) and Δx over time (E), as well as analysis of the Δy from platform per stride in millimeters (F) and Δy over time (G).

(H and I) Analysis of the Δy for the swing-flex phase (H) and the swing-extend phase (I).

(J–L) Analysis of the stride (J), stance (K), and swing duration (L) in milliseconds.

(M) Analysis of cadence.

Each point indicates a single stride. n = 4 aniamls, 7–10 strides/animal OFF trials, n = 7–10 strides/animal ON trials. See Figure S5 and Table S5.

the early- or mid-swing phase, but not the late-swing phase, is able to result in a significant increase in Δy (Figures S5M–S5P).

To assess the impact of the higher Δy in both swing-flex and swing-extend phases during photostimulation, we measured the duration of each stride with or without photostimulation. Although photostimulation of IntA^{Ucn3} neurons results in an increase in stride duration, leading to a decrease in cadence, these changes did not reach statistical significance (Figures 7J–7M, S5G, and S5H). Photostimulation of IntA^{Ucn3} neurons results in consistent changes in hindlimb kinematics (Figures S5Q–S5T), suggesting IntA^{Ucn3} neurons are capable of regulating the hindlimb. In summary, results from the ablation and photostimulation of IntA^{Ucn3} neurons indicate that IntA neurons are necessary and sufficient to control vertical positioning or timing of forelimb movements and ensure the precision of both discrete and rhythmic limb movements.

DISCUSSION

The cerebellum plays an important role in real-time processing of sensory and motor signals for error detection and correction, predictive control, and coordination of limb movements (Ito, 2006), but the functional relevance of the DCN is not well understood. Using a mouse line with previously unknown recombination capability in the cerebellum, we were able to assess the properties and connectivity of a genetically accessible subpopulation of neurons within the IntA. Moreover, we examine the consequences of manipulating these neurons on skilled reach and locomotion. Our results suggest that target selectivity may be a key distinguishing property among neuronal subpopulations in the DCN and illustrate the diversity and complexity of intra- and extra-cerebellar connections made by the DCN. We discuss how IntA neurons ensure accuracy in complex, goal-directed limb movements.

Functional Significance of the Intra- and Extra-cerebellar Connectivity of Neurons in the IntA

Although the cerebellar cortex is organized topographically to some extent, the DCN contains overlapping receptive fields (Uusisaari and De Schutter, 2011). Thus, neuronal subpopulations in the DCN are likely involved in regulation of diverse aspects of movement. The cerebellum integrates sensory information and internal motor commands to refine ongoing motor activity, primarily via cerebello-thalamo-cortical and cerebello-rubro-spinal pathways (Franklin and Wolpert, 2011; Horne and Butler, 1995; Keifer and Houk, 1994). Our results indicate that IntA^{Ucn3} neurons have the ability to influence movement through both pathways, but predominantly project to the cerebello-thalamo-cortical pathway, and that the differential innervation patterns by glutamatergic projection IntA neurons provide means to regulate specific sets of motor activities.

The specificity of intra-cerebellar targets by neurons in the IntA reveals insights to organization and functional significance of these neurons. We observed that IntA^{Ucn3} neurons send NC-MFs primarily to lobules IV to V and the simple lobule, while

other IntA neurons send additional NC-MFs to Crus1 and Crus2 (Figure 3L). Based on delineations by olivo-cortico-nuclear connectivity, these lobules represent the forelimb subdivision of the cerebellum (Voogd et al., 2003). Lobules IV–V and the simple lobule receive MFs from the forelimb and hindlimb through cuneocerebellar and spinocerebellar tracts, respectively, and limited MFs from vestibular and trigeminal nuclei (Altman and Bayer, 1997). In addition, there is a convergence of MFs in lobules I–V from LRt neurons that receive internal copies of motor signals from propriospinal neurons (Alstermark and Ekerot, 2013; Altman and Bayer, 1997; Azim et al., 2014a). Within this general region, lobules I–III receive MFs from the LRt that are carrying information from the hindlimb, whereas lobules IV and V receive MFs that are carrying information from the forelimb (Altman and Bayer, 1997). Thus, the specific targeting of NC-MFs from IntA^{Ucn3} neurons suggests that these neurons represent elements of an internal feedback circuit and relay signals that converge with forelimb movement-related information from the spinal cord to modify these sensory and motor signals.

Mapping the precise extra-cerebellar target regions by IntA^{Ucn3} neurons also provides clues to the nature of their influence. For example, neurons in the VA-VL extensively project to cortical targets, including limb, whisker musculature, and frontal association areas (Kuramoto et al., 2009, 2011); neurons in the CB^{-} zone project to layers II–V, while neurons in the CB^{+} zone project to layer I (Kuramoto et al., 2009). Stimulation of the DCN and VA-VL results in an early excitatory postsynaptic potential response in the deep layers of the primary motor cortex (Yamamoto et al., 1979). Thus, our tract tracing results suggest that IntA^{Ucn3} neurons may influence a fast-conducting class of cortical-projecting VA-VL neurons. In addition, cortical neurons in the CFA of the motor cortex have been demonstrated to selectively activate a short latency effector pathway for the control of skilled reaching movements (Miri et al., 2017). The elucidation of a subset of IntA neurons, which indirectly targets the CFA via VA-VL, provides a specific circuit element through which the IntA may differentially influence patterns of cortical activity and perhaps contribute to the recruitment of motor effector pathways to modulate cortical commands.

Role of the IntA in Coordination of Voluntary Limb Movement

The cerebellum is thought to integrate internally directed copies of motor commands with current sensory status to provide predictive online refinement throughout the movement (Bastian, 2006; Franklin and Wolpert, 2011). DCN neurons, as last-order neurons in the cerebellum, have been implicated in refinement of forelimb movements in goal-oriented behavioral tasks in cat and monkey (Bracha et al., 1999; Küper et al., 2011; Monzée et al., 2004). However, the requirements of distinct components of the cerebellar nuclei for control of forelimb movements have not been examined in mice. The primary challenge lies in the difficulty of specifically targeting neuronal subpopulations within the DCN and the lack of established quantifiable assays for reaching and grasping in mice. Studies describing the kinematics of skilled forelimb movement and locomotion in mice provide the foundation for our interrogation of the role of the DCN in mediating these processes (Azim et al., 2014b; Esposito et al., 2014; Fink et al., 2014; Klein and Dunnett, 2012; Machado et al., 2015). The identification of the *Ucn3*::Cre mouse line presents an opportunity to assess the functional relevance of a neuronal subpopulation in the DCN in behaviorally relevant contexts.

The activities of neurons in the DCN are indirectly linked to muscle control, and stimulation of specific elements of the DCN results in changes in muscle tone (Ebner et al., 2011). In monkey, electrophysiological recordings and stimulation in the Int and dentate/lateral nuclei indicate that activities in these nuclei primarily influence ipsilateral movement (Harvey et al., 1979; MacKay, 1988). In human and cat, recordings and stimulation of the Int nucleus reveal its involvement in activation of flexor and inhibition of extensor muscle activities (Armstrong and Edgley, 1984; Nashold and Slaughter, 1969). Thus, a plausible role for IntA^{Ucn3} neurons is to regulate positioning of forelimb movement in mice through coordination of the ipsilateral flexion movement. Our observation that the absence of IntA^{Ucn3} neurons results in the premature arrival of the limb at the maximum vertical position of the stride suggests IntA^{Ucn3} neurons may participate in gating the onset of flexion (Figure S4R). In support of this notion, analysis of the locomotor kinematics of Purkinje cell degeneration (*Pcd*) mice, a widely used cerebellar disease mouse model, revealed that while stride parameters were not disrupted, the vertical displacement of the forelimb is significantly increased (Machado et al., 2015; Mullen et al., 1976). Together, the selective perturbation in vertical displacement due to loss of Purkinje cells or neurons in the DCN may disrupt coordination of movements across joints within the limb, consistent with patients with cerebellar damage (Bastian et al., 1996).

Representation of movement kinematics is encoded in the DCN (Ebner et al., 2011). It has been long presumed that cerebellar output is necessary for well-timed movements (Ivry et al., 2002), but whether temporal information is encoded in the DCN and how this information is decoded by effectors are not well understood. Besides the activity of Purkinje cells, limited information is available on the role of cerebellar neuronal subtypes in timing of motor events. Recordings in monkeys revealed that activities from the Int and dentate or Lat nuclei precede movements (Thach, 1978), while activity in the fastigial or medial nucleus lags the onset of movement (Bava et al., 1983). In addition, speed and velocity influence neuronal discharge in the Int and dentate/lateral nuclei in cat and monkey (Soechting et al., 1978; van Kan et al., 1993). We show that through the control of onset and extent of forelimb positioning, IntA^{Ucn3} neurons have the ability to influence the timing of limb movements. In addition, the dysmetria-like overreach exhibited by mice lacking IntA^{Ucn3} neurons indicates that these mice are unable to regulate the timing of movement necessary for accurate forelimb targeting, supporting a proposed braking role of the IntA from studies in cats (Ekerot et al., 1997). Consistent with the notion that the cerebellum controls and corrects ongoing motor activities, our study links a subpopulation of glutamatergic IntA neurons and its unique intra- and extra-cerebellar circuitry with coordination of precise and effective movement.

EXPERIMENTAL PROCEDURES

Mouse Strains

C57BL/6JInv (The Jackson Laboratory), *urocortin 3*::Cre (*Ucn3*::Cre; Mutant Mouse Regional Resource Center; Tg[Ucn3-cre]KF31Gsat/Mmucd) (Harris et al., 2014), and *Rosa*::eGFP (B6;129-Gt[ROSA]26Sortm2Sho/J), *Rosa*::lox-stop-lox-ChR2-eYFP (*Ai32*) (B6.Cg-Gt[ROSA]26Sortm32[CAG-COP4*H134R/EYFP]Hze/J), and *Rosa*::lox-stop-lox-hChR2 (H134R)-tdTomato (*Ai27*) (B6.Cg-Gt[ROSA]26Sortm27.1[CAG-COP4*H134R/tdTomato]Hze/J) (The Jackson Laboratory) were obtained. Male and female wild-type and genetically modified mice were used. Adult mice age post-natal day (P) 60 to P120 were used for all experiments. Only heterozygotes were used for each transgene allele. All procedures performed were approved by the NTU/A*STAR Biological Resource Center Institutional Animal Care and Use Committee (IACUC).

Statistics

Comparable numbers of strides per animal of each parameter in control and ablated animals were analyzed to avoid disproportionate effect on the results. Similarly, for photostimulation experiments, equal numbers of strides from each animal during the on and off conditions were used for statistical comparison. Values are represented as mean ± SEM unless otherwise noted. Comparisons were made by unpaired Mann-Whitney U test. Only non-parametric tests were used. The p values for comparisons across more than two groups were calculated using ANOVA. Statistics were analyzed using GraphPad Prism v.7.00 (GraphPad, La Jolla, California, USA). For complete procedures, see Supplemental Information.

SUPPLEMENTAL INFORMATION

Supplemental Information includes Supplemental Experimental Procedures, five figures, five tables, and four movies and can be found with this article online at https://doi.org/10.1016/j.celrep.2018.02.017.

ACKNOWLEDGMENTS

We are grateful to S. Ray for MATLAB scripts and A. Tashiro for *EF1a*::DF-DTR-GFP. We thank C. Koh, H. Ho, and M. Wong for technical assistance. J.N. Betley, T.H. Ch'ng, M. Featherstone, S.H.S. Je, H. Makino, and A. Tashiro provided comments on the manuscript. Work was supported by the Singapore National Medical Research Council (0075/2014) and Singapore Ministry of Education (RG124/15).

AUTHOR CONTRIBUTIONS

A.Y.T.L., A.R.T., A.K.K.Y., and A.I.C. designed the studies and prepared the manuscript, with comments from all authors. A.Y.T.L., A.R.T., and A.K.K.Y. contributed equally to all experiments and analysis of the data and are listed in alphabetical order. K.L.L.W. and M.T. helped with behavioral analysis. J.K. and G.J.A. performed electrophysiological experiments and analyzed the data.

DECLARATION OF INTERESTS

All authors declare no competing financial interests.

Received: August 30, 2017
Revised: November 27, 2017
Accepted: February 2, 2018
Published: February 27, 2018

REFERENCES

Alstermark, B., and Ekerot, C.F. (2013). The lateral reticular nucleus: a precerebellar centre providing the cerebellum with overview and integration of motor functions at systems level. A new hypothesis. J. Physiol. *591*, 5453–5458.

Altman, J., and Bayer, S.A. (1997). Development of the cerebellar system: in relation to its evolution, structure, and functions (CRC Press).

Ankri, L., Husson, Z., Pietrajtis, K., Proville, R., Léna, C., Yarom, Y., Dieudonné, S., and Uusisaari, M.Y. (2015). A novel inhibitory nucleo-cortical circuit controls cerebellar Golgi cell activity. eLife *4*, e06262.

Armstrong, D.M., and Edgley, S.A. (1984). Discharges of nucleus interpositus neurones during locomotion in the cat. J. Physiol. *351*, 411–432.

Azim, E., Fink, A.J., and Jessell, T.M. (2014a). Internal and external feedback circuits for skilled forelimb movement. Cold Spring Harb. Symp. Quant. Biol. *79*, 81–92.

Azim, E., Jiang, J., Alstermark, B., and Jessell, T.M. (2014b). Skilled reaching relies on a V2a propriospinal internal copy circuit. Nature *508*, 357–363.

Bagnall, M.W., Zingg, B., Sakatos, A., Moghadam, S.H., Zeilhofer, H.U., and du Lac, S. (2009). Glycinergic projection neurons of the cerebellum. J. Neurosci. *29*, 10104–10110.

Bastian, A.J. (2006). Learning to predict the future: the cerebellum adapts feedforward movement control. Curr. Opin. Neurobiol. *16*, 645–649.

Bastian, A.J., Martin, T.A., Keating, J.G., and Thach, W.T. (1996). Cerebellar ataxia: abnormal control of interaction torques across multiple joints. J. Neurophysiol. *76*, 492–509.

Bava, A., Grimm, R.J., and Rushmer, D.S. (1983). Fastigial unit activity during voluntary movement in primates. Brain Res. *288*, 371–374.

Beitzel, C.S., Houck, B.D., Lewis, S.M., and Person, A.L. (2017). Rubrocerebellar feedback loop isolates the interposed nucleus as an independent processor of corollary discharge information in mice. J. Neurosci. *37*, 10085–10096.

Bostan, A.C., Dum, R.P., and Strick, P.L. (2013). Cerebellar networks with the cerebral cortex and basal ganglia. Trends Cogn. Sci. *17*, 241–254.

Bracha, V., Kolb, F.P., Irwin, K.B., and Bloedel, J.R. (1999). Inactivation of interposed nuclei in the cat: classically conditioned withdrawal reflexes, voluntary limb movements and the action primitive hypothesis. Exp. Brain Res. *126*, 77–92.

Chan-Palay, V. (1977). Cerebellar dentate nucleus: organization, cytology and transmitters (Springer-Verlag).

Chung, S.H., Marzban, H., and Hawkes, R. (2009). Compartmentation of the cerebellar nuclei of the mouse. Neuroscience *161*, 123–138.

De Schutter, E., and Bjaalie, J.G. (2001). Coding in the granular layer of the cerebellum. Prog. Brain Res. *130*, 279–296.

Ebner, T.J., Hewitt, A.L., and Popa, L.S. (2011). What features of limb movements are encoded in the discharge of cerebellar neurons? Cerebellum *10*, 683–693.

Eccles, J.C., Ito, M., and Szentágothai, J. (1967). The cerebellum as a neuronal machine (Springer-Verlag).

Ekerot, C.F., Garwicz, M., and Jörntell, H. (1997). The control of forelimb movements by intermediate cerebellum. Prog. Brain Res. *114*, 423–429.

Engberg, I., and Lundberg, A. (1969). An electromyographic analysis of muscular activity in the hindlimb of the cat during unrestrained locomotion. Acta Physiol. Scand. *75*, 614–630.

Esposito, M.S., Capelli, P., and Arber, S. (2014). Brainstem nucleus MdV mediates skilled forelimb motor tasks. Nature *508*, 351–356.

Fink, A.J., Croce, K.R., Huang, Z.J., Abbott, L.F., Jessell, T.M., and Azim, E. (2014). Presynaptic inhibition of spinal sensory feedback ensures smooth movement. Nature *509*, 43–48.

Franklin, D.W., and Wolpert, D.M. (2011). Computational mechanisms of sensorimotor control. Neuron *72*, 425–442.

Gao, Z., Proietti-Onori, M., Lin, Z., Ten Brinke, M.M., Boele, H.J., Potters, J.W., Ruigrok, T.J., Hoebeek, F.E., and De Zeeuw, C.I. (2016). Excitatory cerebellar nucleocortical circuit provides internal amplification during associative conditioning. Neuron *89*, 645–657.

Harris, J.A., Hirokawa, K.E., Sorensen, S.A., Gu, H., Mills, M., Ng, L.L., Bohn, P., Mortrud, M., Ouellette, B., Kidney, J., et al. (2014). Anatomical

characterization of Cre driver mice for neural circuit mapping and manipulation. Front. Neural Circuits *8*, 76.

Harvey, R.J., Porter, R., and Rawson, J.A. (1979). Discharges of intracerebellar nuclear cells in monkeys. J. Physiol. *297*, 559–580.

Heiney, S.A., Kim, J., Augustine, G.J., and Medina, J.F. (2014). Precise control of movement kinematics by optogenetic inhibition of Purkinje cell activity. J. Neurosci. *34*, 2321–2330.

Hioki, H., Fujiyama, F., Taki, K., Tomioka, R., Furuta, T., Tamamaki, N., and Kaneko, T. (2003). Differential distribution of vesicular glutamate transporters in the rat cerebellar cortex. Neuroscience *117*, 1–6.

Horne, M.K., and Butler, E.G. (1995). The role of the cerebello-thalamo-cortical pathway in skilled movement. Prog. Neurobiol. *46*, 199–213.

Houck, B.D., and Person, A.L. (2015). Cerebellar premotor output neurons collateralize to innervate the cerebellar cortex. J. Comp. Neurol. *523*, 2254–2271.

Ito, M. (2006). Cerebellar circuitry as a neuronal machine. Prog. Neurobiol. *78*, 272–303.

Ivry, R.B., Spencer, R.M., Zelaznik, H.N., and Diedrichsen, J. (2002). The cerebellum and event timing. Ann. N Y Acad. Sci. *978*, 302–317.

Keifer, J., and Houk, J.C. (1994). Motor function of the cerebellorubrospinal system. Physiol. Rev. *74*, 509–542.

Klein, A., and Dunnett, S.B. (2012). Analysis of skilled forelimb movement in rats: the single pellet reaching test and staircase test. Curr. Protoc. Neurosci. *58*, 8.28.1–8.28.15.

Küper, M., Hermsdörfer, J., Brandauer, B., Thürling, M., Schoch, B., Theysohn, N., and Timmann, D. (2011). Lesions of the dentate and interposed nuclei are associated with impaired prehension in cerebellar patients. Neurosci. Lett. *499*, 132–136.

Kuramoto, E., Furuta, T., Nakamura, K.C., Unzai, T., Hioki, H., and Kaneko, T. (2009). Two types of thalamocortical projections from the motor thalamic nuclei of the rat: a single neuron-tracing study using viral vectors. Cereb. Cortex *19*, 2065–2077.

Kuramoto, E., Fujiyama, F., Nakamura, K.C., Tanaka, Y., Hioki, H., and Kaneko, T. (2011). Complementary distribution of glutamatergic cerebellar and GABAergic basal ganglia afferents to the rat motor thalamic nuclei. Eur. J. Neurosci. *33*, 95–109.

Lee, K.H., Mathews, P.J., Reeves, A.M., Choe, K.Y., Jami, S.A., Serrano, R.E., and Otis, T.S. (2015). Circuit mechanisms underlying motor memory formation in the cerebellum. Neuron *86*, 529–540.

Lefler, Y., Yarom, Y., and Uusisaari, M.Y. (2014). Cerebellar inhibitory input to the inferior olive decreases electrical coupling and blocks subthreshold oscillations. Neuron *81*, 1389–1400.

Leto, K., Carletti, B., Williams, I.M., Magrassi, L., and Rossi, F. (2006). Different types of cerebellar GABAergic interneurons originate from a common pool of multipotent progenitor cells. J. Neurosci. *26*, 11682–11694.

Machado, A.S., Darmohray, D.M., Fayad, J., Marques, H.G., and Carey, M.R. (2015). A quantitative framework for whole-body coordination reveals specific deficits in freely walking ataxic mice. eLife *4*, e07892.

MacKay, W.A. (1988). Cerebellar nuclear activity in relation to simple movements. Exp. Brain Res. *71*, 47–58.

Miri, A., Warriner, C.L., Seely, J.S., Elsayed, G.F., Cunningham, J.P., Churchland, M.M., and Jessell, T.M. (2017). Behaviorally selective engagement of short-latency effector pathways by motor cortex. Neuron *95*, 683–696.

Monzée, J., Drew, T., and Smith, A.M. (2004). Effects of muscimol inactivation of the cerebellar nuclei on precision grip. J. Neurophysiol. *91*, 1240–1249.

Mullen, R.J., Eicher, E.M., and Sidman, R.L. (1976). Purkinje cell degeneration, a new neurological mutation in the mouse. Proc. Natl. Acad. Sci. USA *73*, 208–212.

Najac, M., and Raman, I.M. (2017). Synaptic excitation by climbing fibre collaterals in the cerebellar nuclei of juvenile and adult mice. J. Physiol. *595*, 6703–6718.

Nashold, B.S., Jr., and Slaughter, D.G. (1969). Effects of stimulating or destroying the deep cerebellar regions in man. J. Neurosurg. *31*, 172–186.

Paxinos, G., and Franklin, K.B.J. (2007). The Mouse Brain in Stereotaxic Coordinates, Third Edition (Elsevier Academic Press).

Shemesh, Y., Forkosh, O., Mahn, M., Anpilov, S., Sztainberg, Y., Manashirov, S., Shlapobersky, T., Elliott, E., Tabouy, L., Ezra, G., et al. (2016). Ucn3 and CRF-R2 in the medial amygdala regulate complex social dynamics. Nat. Neurosci. *19*, 1489–1496.

Soechting, J.F., Burton, J.E., and Onoda, N. (1978). Relationships between sensory input, motor output and unit activity in interpositus and red nuclei during intentional movement. Brain Res. *152*, 65–79.

Tennant, K.A., Adkins, D.L., Donlan, N.A., Asay, A.L., Thomas, N., Kleim, J.A., and Jones, T.A. (2011). The organization of the forelimb representation of the C57BL/6 mouse motor cortex as defined by intracortical microstimulation and cytoarchitecture. Cereb. Cortex *21*, 865–876.

Teune, T.M., van der Burg, J., van der Moer, J., Voogd, J., and Ruigrok, T.J. (2000). Topography of cerebellar nuclear projections to the brain stem in the rat. Prog. Brain Res. *124*, 141–172.

Thach, W.T. (1978). Correlation of neural discharge with pattern and force of muscular activity, joint position, and direction of intended next movement in motor cortex and cerebellum. J. Neurophysiol. *41*, 654–676.

Tolbert, D.L., Bantli, H., and Bloedel, J.R. (1978). Organizational features of the cat and monkey cerebellar nucleocortical projection. J. Comp. Neurol. *182*, 39–56.

Uusisaari, M., and De Schutter, E. (2011). The mysterious microcircuitry of the cerebellar nuclei. J. Physiol. *589*, 3441–3457.

Uusisaari, M., and Knöpfel, T. (2011). Functional classification of neurons in the mouse lateral cerebellar nuclei. Cerebellum *10*, 637–646.

Uusisaari, M., Obata, K., and Knöpfel, T. (2007). Morphological and electrophysiological properties of GABAergic and non-GABAergic cells in the deep cerebellar nuclei. J. Neurophysiol. *97*, 901–911.

van Kan, P.L., Houk, J.C., and Gibson, A.R. (1993). Output organization of intermediate cerebellum of the monkey. J. Neurophysiol. *69*, 57–73.

Voogd, J., Pardoe, J., Ruigrok, T.J., and Apps, R. (2003). The distribution of climbing and mossy fiber collateral branches from the copula pyramidis and the paramedian lobule: congruence of climbing fiber cortical zones and the pattern of zebrin banding within the rat cerebellum. J. Neurosci. *23*, 4645–4656.

Witter, L., Canto, C.B., Hoogland, T.M., de Gruijl, J.R., and De Zeeuw, C.I. (2013). Strength and timing of motor responses mediated by rebound firing in the cerebellar nuclei after Purkinje cell activation. Front. Neural Circuits *7*, 133.

Yamamoto, T., Kawaguchi, S., and Samejima, A. (1979). Electrophysiological studies on the cerebellocerebral projection in the rat. Exp. Neurol. *63*, 545–558.

Zainolabidin, N., Kamath, S.P., Thanawalla, A.R., and Chen, A.I. (2017). Distinct activities of Tfap2A and Tfap2B in the specification of GABAergic interneurons in the developing cerebellum. Front. Mol. Neurosci. *10*, 281.